Chinese Chemical Letters 34 (2023) 107465

Contents lists available at ScienceDirect

Chinese Chemical Letters

journal homepage: www.elsevier.com/locate/cclet

Tea-derived carbon materials as anode for high-performance sodium ion batteries

Huayan Wang[a,b,1], Huixin Chen[b,f,1], Chi Chen[b,f], Miao Li[c], Yiming Xie[a,*], Xingcai Zhang[d,e], Xianwen Wu[g], Qiaobao Zhang[c,*], Canzhong Lu[b,f,**]

[a] Engineering Research Center of Environment-Friendly Function Materials, Ministry of Education, Institute of Materials Physical Chemistry, Huaqiao University, Xiamen 361021, China
[b] CAS key Laboratory of Design and Assembly of Functional Nanostructures, and Fujian Provincial Key Laboratory of Nanomaterials, Fujian Institute of Research on the Structure of Matter, Chinese Academy of Sciences, Fuzhou 350002, China
[c] Department of Materials Science and Engineering, College of Materials, Xiamen University, Xiamen 361005, China
[d] School of Engineering and Applied Sciences, Harvard University, Cambridge, MA 02138, United States
[e] School of Engineering, Massachusetts Institute of Technology, Cambridge, MA 02139, United States
[f] Xiamen Key Laboratory of Rare Earth Photoelectric Functional Materials, Xiamen Institute of Rare Earth Materials, Haixi Institutes, Chinese Academy of Sciences, Xiamen 361021, China
[g] School of Chemistry and Chemical Engineering, Jishou University, Jishou 416000, China

ARTICLE INFO

Article history:
Received 17 March 2022
Revised 21 April 2022
Accepted 23 April 2022
Available online 29 April 2022

Keywords:
Tea tomenta
Co-doped
Hard carbon
Initial coulombic efficiency
Sodium-ion batteries

ABSTRACT

Sodium-ion batteries (SIB) have attracted widespread attention in large-scale energy storage fields owing to the abundant reserve in the earth and similar properties of sodium to lithium. Biomass-based carbon materials with low-cost, controllable structure, simple processing technology, and environmental friendliness tick almost all the right boxes as one of the promising anode materials for SIB. Herein, we present a simple novel strategy involving tea tomenta biomass-derived carbon anode with enhanced interlayer carbon distance (0.44 nm) and high performance, which is constructed by N,P co-doped hard carbon (Tea-1100-NP) derived from tea tomenta. The prepared Tea-1100-NP composite could deliver a high reversible capacity (326.1 mAh/g at 28 mA/g), high initial coulombic efficiency (ICE = 90% at 28 mA/g), stable cycle life (262.4 mAh/g at 280 mA/g for 100 cycles), and superior rate performance (224.5 mAh/g at 1400 mA/g). Experimental results show that the excellent electrochemical performance of Tea-1100-NP due to the high number of active N,P-containing groups, and disordered amorphous structures provide ample active sites and increase the conductivity, meanwhile, large amounts of microporous shorten the Na^+ diffusion distance as well as quicken ion transport. This work provides a new type of N,P co-doped high-performance tomenta-derived carbon, which may also greatly promote the commercial application of SIB.

© 2023 Published by Elsevier B.V. on behalf of Chinese Chemical Society and Institute of Materia Medica, Chinese Academy of Medical Sciences.

With the development of social economy, people's demand for energy continues to grow. The massive consumption of traditional fossil energy has caused problems such as global temperature rise and environmental degradation, which have threatened the survival of mankind. In this situation, striving to achieve "carbon neutrality" and the development of renewable energy and energy storage technologies have become the top priority [1,2]. As a type of energy storage technology with high energy density, lithium-ion batteries (LIB) have been widely used in large-scale energy storage systems such as electric vehicles and smart grids [3,4]. However, the reserves of lithium are limited (the abundance of lithium reserves is 0.0065%) and unevenly distributed, a large amount of demand causes a shortage of lithium resources and price increases, which may make it difficult for global lithium resources to meet the ever-increasing demand [5–7]. Therefore, there is an urgent need to develop a new low-cost, high-performance energy storage battery system. Compared with the lithium, the sodium of the same main group has obvious advantages of abundant reserves, similar electrochemical properties

* Corresponding authors.
** Corresponding author at: CAS key Laboratory of Design and Assembly of Functional Nanostructures, and Fujian Provincial Key Laboratory of Nanomaterials, Fujian Institute of Research on the Structure of Matter, Chinese Academy of Sciences, Fuzhou 350002, China.
E-mail addresses: ymxie@hqu.edu.cn (Y. Xie), zhangqiaobao@xmu.edu.cn (Q. Zhang), czlu@fjirsm.ac.cn (C. Lu).
[1] These authors contributed equally to this work.

https://doi.org/10.1016/j.cclet.2022.04.063
1001-8417/© 2023 Published by Elsevier B.V. on behalf of Chinese Chemical Society and Institute of Materia Medica, Chinese Academy of Medical Sciences.

and lower prices, therefore, sodium-ion batteries (SIB) can be used as a substitute for large-scale energy storage of LIB [8–12]. In recent years, an important reason hindering the rapid development the commercialization of SIB is the lack of suitable anode materials [13–15]. Therefore, the development of high-performance anode materials is becoming a research focus and focus at this stage.

Hard carbon have attracted wide-ranging attention due to their controllable structure, low cost, excellent cycle stability, good electrochemical properties, safety performance, and meet the requirements of large-scale energy storage [16]. As a kind of hard carbon, the good geometry, hierarchical structure, conductivity, stability and safety of biomass-based carbon make it one of the most promising anode electrode candidates for SIB. In nature, biomass materials usually exhibit a wide variety of macroscopic structures. Especially, porous carbon and carbon-derived materials contain a large specific surface area that can be easily obtained by simple calcination, which are beneficial to improve reaction kinetics and electronic conductivity [17–19]. The main problems faced by the current anode electrode materials are low capacity, poor rate performance, and low ICE. In response to these problems, researchers have proposed a variety of solutions to continuously improve sodium storage performance. Wu *et al.* [20] obtained a lotus seed pod-derived hard carbon material exhibited a reversible capacity of 328.8 mAh/g at a current density of 50 mA/g. However, 50% of ICE still does not meet the requirements of commercially available anode materials. Xie *et al.* [21] obtained a carbon dot from the supernatant of hydrothermal carbonization as anodes for SIB exhibit an excellent specific capacity of over 300 mAh/g with a significantly enhanced ICE of up to 91% at 30 mA/g. However, the synthesis process of such hard carbon with ultra-high ICE is very complicated, high in cost, and will be more difficult to apply in commercial practical use. Heteroatom doped has also proved to be an effective method to provide additional reaction sites for sodium ion storage to improve electrochemical performance [22–24]. Compared with single-atom doped, the synergistic effect of co-doped with multiple heteroatoms can more effectively improve the sodium storage performance of carbon materials [25,26]. These modification methods have improved the reversible specific capacity and ICE, but still fail to meet the requirements [27–30]. The optimization goals of hard carbon anodes include improving specific capacity, ICE, rate performance and long-cycle stability, but these goals often conflict with each other and are difficult to balance [31]. Therefore, it is necessary to explore a hard carbon material with high specific capacity, high ICE, excellent rate performance and cycle performance.

In this work, we designed a N,P co-doped hard carbon from tea tomenta (Tea-1100-NP) with a large interlayer spacing and an appropriate specific surface area. The electrode exhibits a high reversible capacity of 326.1 mAh/g and high ICE of 90% at a current density of 28 mA/g. At the same time, Tea-1100-NP has super stable Na^+ storage performance, delivered a specific capacity of 262.4 mAh/g at a high specific current of 280 mA/g after 100 cycles. Even at a large current density of 1400 mA/g, the reversible capacity of 224.5 mAh/g can be maintained.

Tea-1100: The tea was purchased from Bama Tea Co., Ltd. (China). First, the tea was thoroughly separated by standard wire sieves (0.3 mm), and the tomenta on the standard wire was cleaned by deionized water and ethanol. Then, the sample was heated in 1 mol/L HCl at 120 °C for 3 h to completely remove the residual impurities. Next, the sample was washed with deionized water before being dried at 80 °C overnight in a vacuum oven. Finally, the sample was deposited in a porcelain boat and precarbonized at 600 °C for 2 h and then carbonized 1100 °C for 3 h with a heating rate of 5 °C/min in flowing Ar atmosphere to obtain the product named Tea-1100.

Tea-1100-NP: The dried Tea-1100 (1 g) and melamine (2.5 g) were added into a round-bottomed flask with deionized water (1 L) and stir 20 h. Afterward, phytic acid (10 mL) was added into and kept stirring 6 h, followed by drying at 80 °C overnight in a vacuum oven. Finally, the obtained sample was carbonized at 700 °C for 2 h at an initial heating rate of 5 °C/min in flowing Ar.

Thermogravimetric analysis (TGA) was carried out on a Mettler-Toledo TGA/DSC 1, 10 °C/min under air atmosphere. The morphologies of the samples were characterized with scanning electron microscopy (SEM, Apreo S), transmission electron microscopy (TEM, FEI Tecnai F20) and high-resolution transmission electron microscopy (HRTEM, JEOL JEM 2100F). The structures of the samples were measured by X-ray diffraction (XRD, Rigaku Miniflex 600) using Cu K-Alpha radiation ($\lambda = 0.15406$ nm), and Raman spectrometry (RENISHAW inVia) using a laser with a wavelength of 532 nm. The FTIR spectra were obtained with a Fourier transform infrared spectrometer (FTIR, Bruker VERTEX 70 & ALPHA). The specific surface area was calculated by nitrogen adsorption isotherms according to the Brunauer-Emmett-Teller (BET) method, which was obtained by an argon adsorption apparatus (Micromeritics ASAP2020 Version 4.03) at 87 K. The surface properties were confirmed by X-ray photoelectron spectroscopies (XPS, Thermo Scientific K-Alpha), which were measured using an image photoelectron spectrometer with Al K-Alpha X-ray source.

Electrochemical performance of active material as anode for SIBs was conducted at 30 °C using 2025-type coin cells with sodium metal as the counter electrode, 1.0 mol/L $NaCF_3SO_3$ in diethylene glycol dimethyl ether (DEGDME) as electrolyte, and glass fiber as the separator. The working electrodes were composed of a mixture with 80 wt% active material, 10 wt% super P conductive carbon, 10 wt% sodium carboxymethyl cellulose (CMC) binder, which were firstly dispersed in deionized water to make slurry and casted on aluminum foil, dried and cut into a disk with a diameter of 14 mm. All the cells were assembled in an argon-filled glove box with $[O_2]$ and $[H_2O] \leq 0.1$ ppm.

Discharge and charge measurements at different current densities were performed in the voltage range of 0.01–3.0 V on a battery testing system (Shenzhen Neware, China). Cyclic voltammetry (CV), linear sweep voltammetry (LSV) and electrochemical impedance spectroscopy (EIS) were performed by electrochemical workstation (Shanghai Chenhua CHI 760e, China), CV measurements were conducted at various scan rates from 0.1 mV/s to 1 mV/s, LSV was obtained through a single sweep in the potential sweep range of −0.06 V to 0.06 V and the EIS was carried out with a voltage amplitude of 10 mV in frequency range of 100 kHz to 0.1 Hz. Galvanostatic intermittent titration technique (GITT) was in the electrodes at a specific current of 280 mA/g and a current pulse time of 2 min at 1 h intervals.

The overall synthesis strategy of Tea-1100 and Tea-1100-NP is shown in Fig. 1. After sieving the tea, the tomenta is taken, and the precursor is formed after the tomenta is treated by acid. Then, the precursor is carbonized and the carbon skeleton was effectively doped with N, P atoms to form porous hard carbon with extended interlayer spacing. Meanwhile, in order to study the formation process of tomenta hard carbon, the carbonization process of tomenta in air atmosphere was analyzed by TGA. As we all know, the process of biomass pyrolysis can generally be divided into three stages: water evaporation, branched chain breakage and recombination, and aromatic ring condensation to carbon [32,33]. As demonstrated in Fig. S1 (Supporting information), the tea has a mass loss rate of 6.1% from room temperature to ~240 °C, which can be attributed to the loss of physically and chemically adsorbed water molecules and light volatile compounds. From 240 °C to 433 °C, the mass loss is 72.1%, which may be the cause of the formation of organic carbon. From 433 °C to 529 °C, the mass loss is 11.9%, which may be related to the combustion and de-

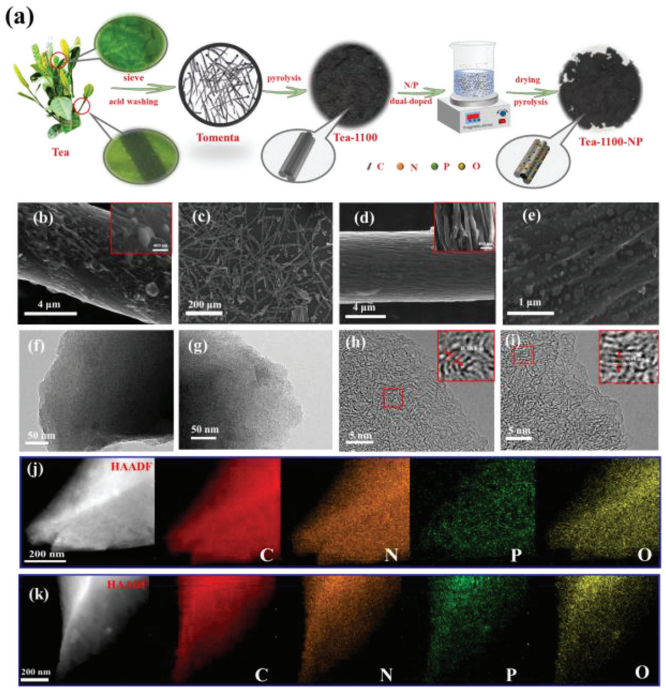

Fig. 1. (a) Schematic illustration of the material synthesis process of Tea-1100 and Tea-1100-NP. SEM images of (b) Tea-1100, (c–e) Tea-1100-NP. TEM images of (f) Tea-1100, (g) Tea-1100-NP. HRTEM images of (h) Tea-1100, (i) Tea-1100-NP. Elemental mappings of (j) Tea-1100, (k) Tea-1100-NP. The insets of (b, d, h, i) are corresponding enlarged images.

volatilization of organic carbon. The remaining 9.9% is inorganic residue. The Tea-1100-untreated (tomenta without HCl treatment are carbonized at 1100 °C), Tea (uncarbonized tomenta), Tea-1100 and Tea-1100-NP, the residues after combustion are 11%, 9%, 5.2% and 2.6%. Observing the TGA curve clearly shows that acid washing can remove the residual impurities and increase the carbon ratio [34,35], and the introduction of N, P atoms can also improve the carbonization yield of sample due to the rich in C elements in the phytic acid and melamine.

The SEM characterization (Figs. 1b–e) presents that all sample exhibit rod-like fiber morphology. This unique rod-like morphology is likely formed from broken tomenta, and the rod lengths range from 20 μm to 600 μm. Observing the single rod-shaped, it was found that the surface exhibited an irregular strip appearance, where it provides a suitable space for diffusion, penetration of the electrolyte solution. Furthermore, the surface state of Tea-1100 is similar to that of Tea-1100-NP, indicating that N,P co-doped has a relatively small effect on the surface structure of the materials. To further confirm the morphology, we provide the TEM image. The TEM images of Tea-1100 and Tea-1100-NP (Figs. 1f–i) presents that such a lamellar carbon sheet was composed of non-uniform dense particles loosely packed in the rugged surface, such a loose and lamellar structure is highly beneficial to electrochemical Na^+ adsorption/desorption process. But, as shown by TEM of tea in Figs. S2a and b (Supporting information), the surface of tea that has not been carbonized is almost smooth. It also presents a rod shape, a slight local strip surface. It can be seen from the HRTEM photograph shown in Fig. 1j that all samples belong to amorphous domains with disordered structure. Among them, the introduction of N, P atoms is out of shape the carbon sheet, forming evident flaws and nano-interspaces. Further measurement of the carbon layer spacing of the all samples reveals that the carbon layer spacing of Tea-1100-NP is significantly larger than that of Tea-1100, which is due to the introduction of P atoms with a larger atomic radius, which deforms the carbon sheet structure [28,36]. Thereby the average layer spacing of Tea-1100-NP (0.44 nm) is wider than that of Tea-1100 (0.38 nm), but both are much larger than that of graphite (0.34 nm), which is considered to be advantageous for Na^+ intercalation-deintercalation [37]. Furthermore, the element mapping images in Fig. 1k indicate that the carbonization of the tomenta will form oxygen atom self-doped hard carbon, and it also reveals that the C, N, P, O elements were uniformly distributed in the sample powder.

In order to further study the physical properties of carbon materials, XRD patterns were carried out. As shown in Fig. 2a, the XRD patterns of all samples show two broad and scattered peaks at around 22° (002) and 42° (100), which indicates that all samples are disordered amorphous structures. Shaped carbon generates a very small amount of crystalline carbon during the carbonization process. Compared with amorphous carbon, the proportion of excess crystalline carbon is very small, which can be ignored to a large extent and will not affect the conclusion [22]. Compared with Tea-1100, Tea-1100-NP has a weaker diffraction peak on the (100) crystal plane, indicating that its crystallinity is decreasing. With the introduction of phytic acid and melamine, the diffraction peak of the (002) crystal plane gradually shifted to a low angle, indicating that the interlayer spacing was significantly increased, this phenomenon was attributed to the introduction of heteroatoms, which is consistent with the TEM observation result. The broad feature of the peak is due to the porous structure, which reduces the crystallization of the graphite wall. In order to better observe the influence of the introduction of N, P atoms on the structure of carbon materials, Raman spectroscopy was further applied to the structure of the hard carbon produced in the study. As shown in Fig. 2b, all samples can be observed that two typical peaks are located at 1347 cm^{-1} and 1582 cm^{-1}. The half-width of the D peak of Tea-1100-NP becomes larger, and the peak position moves slightly to the direction of low wave number, which proves the existence of N, P doped. According to calculations, the I_D/I_G ratios of Tea-1100-NP and Tea-1100 are 1.98 and 1.73, respectively (Table 1), which shows that Tea-1100-NP has more edge defects and structural deformations than Tea-1100. It also proves N, P co-doped can promote the amorphous structure of carbon materials and produce more defects, which is consistent with the XRD results. The FT-IR curve of Tea-1100 and Tea-1100-NP (Fig. 2c) confirmed the successful conversion of tomenta to carbon and the completion of heteroatom doped. Several typical absorption peaks at 1620 and 3400 cm^{-1} are observed in the film electrode, which are corresponding to characteristic absorption peaks of the C=O and O–H groups, respectively [38]. Special attention is required that we can observe that the carbonyl group content of Tea-1100-NP is increased compared to Tea-1100. The pore structure and BET specific surface area of the two samples were evaluated by N_2 adsorption-desorption measurement. As shown in Fig. 2d, the N_2 adsorption and desorption curve is not closed. This is because the pores of carbon materials are mostly flexible pores or pores that are only accessible *via* small necks, and the diameter of the pores shrinks after gas adsorption, which makes the adsorbed gas difficult to desorb, thereby inhibiting the equilibrium desorption of the gas, resulting in an unclosed adsorption and desorption curve [39]. Observing the pore size distribution map estimated by the Barrett-Joyner-Halenda (BJH) model (Fig. 2e), the results show that the tomenta-derived carbon material is a hierarchical porous material. According to IUPAC, the hysteresis loop can be divided into four types, Tea-1100 and Tea-1100-NP both show hysteresis, the hysteresis loop conforms to type IV isotherm [40], the BET surface area are 39.78 m^2/g and 13.92 m^2/g, respectively (Table 1), the larger specific surface area makes the electrolyte and the electrode completely contact, which is conducive to the migration and transmission of sodium ions and electrons. Therefore, increasing the specific surface area of

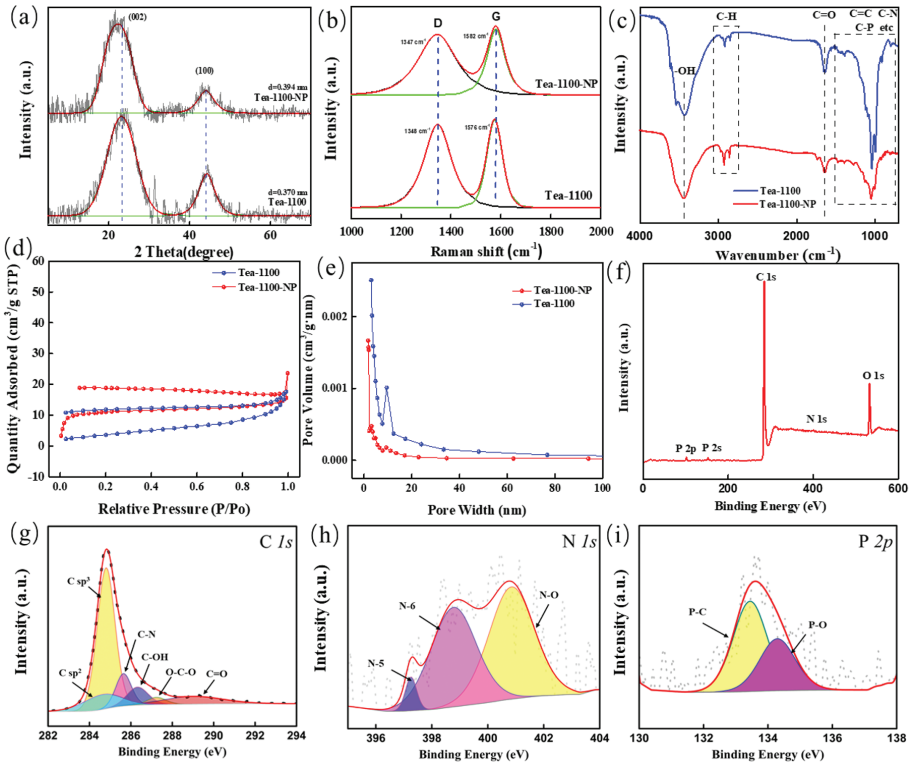

Fig. 2. Tea-1100 and Tea-1100-NP of (a) XRD patterns and (b) Raman spectra. (c) FTIR spectra of Tea-1100-NP. Tea-1100 and Tea-1100-NP of (d) N_2 adsorption/desorption isotherms and (e) BJH pore size distributions. Tea-1100-NP of (f) XPS survey spectra, (g) High-resolution C 1s spectra, (h) High-resolution N 1s spectra, (i) High-resolution P 2p spectra.

Table 1
Structure parameters and results of deconvoluting the N 1s and P 2p peaks of the Tea-1100 and Tea-1100-NP.

Samples	I_D/I_G	S_{BET} (m^2/g)	Pore volume (cm^3/g)	Composition (%)				N 1s bondscontents (%)			P 2p bondscontents (%)	
				C	O	N	P	N-6	N-5	N–O	P–C	P–O
Tea-1100	1.73	13.92	0.02	90.85	8.55	0.48	0.11	9.22	43.13	47.65	41.24	58.76
Tea-1100-NP	1.98	39.78	0.03	88.28	10.24	0.83	0.75	3.62	54.34	42.04	70.91	29.09

biomass porous carbon also helps to increase the reversible capacity. However, the lower specific surface area can reduce side reactions and the formation of solid electrolyte interface (SEI), thereby improving ICE, which is consistent with subsequent electrochemical results. Therefore, after proper trace doped, Tea-1100 forms Tea-1100-NP with a larger surface area. At the same time, the specific surface area of Tea-1100-NP is not too high, not only can increase the contact between the electrolyte and the electrode, but also reduce the side reactions and the formation of SEI. The pore volume of Tea-1100 is 0.02 cm^3/g, while the pore volume of Tea-1100-NP is 0.03 cm^3/g (Table 1). It mainly contains two kinds of nano-pores of 1.78 and 2.03 nm, this rich hierarchical porous structure can ensure sufficient electrolyte penetration, increase the diffusion rate of Na^+, and even slow down the volume change during the sodiation/desodiation process. The abundant micropores in the structure can provide more sodium storage locations and avoid excessive electrolyte decomposition. At the same time, the presence of micropores increases the specific surface area and provides sufficient electrode/electrolyte interface for the accumulation of ions or charges. In addition, the pore structure of the carbon material is slightly changed due to the introduction of heteroatoms N, P, which is consistent with the results of XRD.

In order to further understand the composition characteristics and element distribution of all samples, XPS analysis was carried out. As shown in Table 1, C, O, N, P elements were present in all samples, and their contents are 88.28%, 10.24%, 0.83% and 0.75%. The XPS further confirmed that N, P atoms have been successfully doped into the C skeleton, the phytic acid and melamine introduced during the preparation process make the N, P, O content of Tea-1100-NP higher than that of Tea-1100. The XPS total spectrum (Fig. 2f) of Tea-1100-NP shows a sharp peak (285 eV) and four weak peaks (399, 532, 154 and 102 eV), corresponding to the peaks of C 1s, N 1s, O 1s and P 2p, respectively. The XPS spectrum of Tea-1100 also shows similar C, N, O, P element peaks (Fig. S3a in Supporting information). In order to determine the bond composition of each element, C 1s, N 1s and P 2p are peaked according to the binding energy of different bonds. First, as shown in Fig. 2g, the C 1s of Tea-1100-NP can be fitted to six peaks: C–C(sp^2), C–C(sp^3), C–N, C–O, C=O and O–C–O. Second, N can be divided into three types, as shown in Fig. 2h and Fig. S3b (Supporting information): pyridine nitrogen (N-6, 397.5 eV), pyrrole nitrogen (N-5, 398.5 eV) and oxidizing nitrogen (N–O, 401.5 eV), the corresponding content ratios of the three N elements are listed in Table 1. The defect sites generated by N-6 and N-5 increase the disorder and conductivity of carbon, which can improve the storage performance of Na^+ [41,42]. As shown in Table 1, the total content ratio of N-6 and N-5 in Tea-1100-NP is 57.96%, which is higher than Tea-1100 (52.35%). Therefore, compared with Tea-1100, Tea-1100-NP has higher disorder and conductivity (Fig. S4 in Supporting information) [43,44], which is consistent with the Raman results. Finally, as shown in

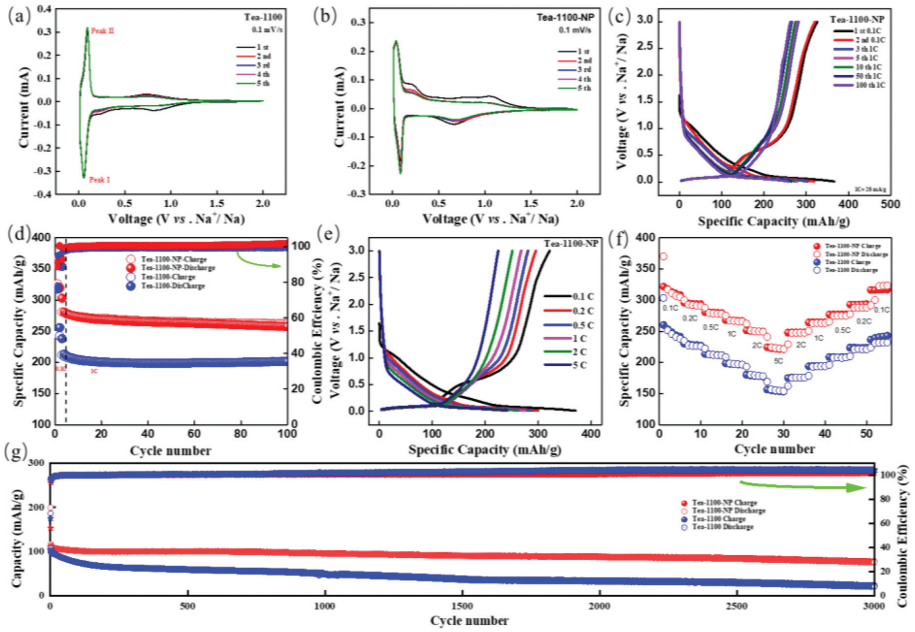

Fig. 3. CV curves at 0.1 mV/s of (a) Tea-1100, (b) Tea-1100-NP. Tea-1100-NP of (c) initial GCD curves at 1 C, the electrode was first tested at 0.1 C for two cycles. (d) Cycle performance at 1 C, the electrode was first tested at 0.1 C for two cycles and then subjected to long-term cycling. (e) GCD profiles at different current densities. (f) Rate performance at various current densities. (g) Cycle performance at 5 A/g.

Fig. 2i and Fig. S3c (Supporting information), the P 2p spectrum can be fitted to two peaks, the main peak is around 133.5 eV, and the small peak is around 34.5 eV, which are attributed to the P–C bond and the P–O bond, respectively. The corresponding content ratios are listed in Table 1. The appearance of C–P and C–N peaks proved that N, P atoms were successfully injected into the carbon lattice, the introduction of N atoms can induce defects, while the introduction of P atoms usually triggers the deformation of the graphite sheet, both can produce more activity site [45].

Therefore, in this work, the prepared tomenta-derived carbon material is used as the anode of SIB, and detailed electrochemical behavior analysis is carried out on it. The CV curve shown in Figs. 3a and b are the first 5 cycles at 0.1 mV/s. In the first cycle of Tea-1100, a broad reduction peak appeared near 0.82 V, which was attributed to the irreversible reaction between the surface functional groups of the carbon material and the electrolyte [46]; N, P doped in the latter Tea-1100-NP, a similar irreversible reduction peak can be detected, but its position is slightly shifted to 0.23 V, indicating that part of the N, P in Tea-1100-NP participates in the irreversible reaction. Another small irreversible reduction peak appeared near 1.02 V, which disappeared in the subsequent scan, which can be attributed to the formation of the SEI layer. However, due to the low surface area of carbon, we believe that these two peaks are more of an irreversible Na^+ intercalation process. These two reduction peaks disappeared in the subsequent cycles, indicating that the material is only about 90% of the ICE can be explained by the formation of the SEI layer and the side reaction of the surface functional groups during the first discharge. There is a significant redox reaction near 0.01/0.1 V, which usually indicates that Na^+ has more obvious intercalation and delamination behavior in the electrochemical reaction. Tea-1100 and Tea-1100-NP have a pair of weak redox peaks around 0.75 V and 0.67 V, respectively, which may be related to the redox reaction on the surface of the functionalized carbon electrode, in the subsequent CV cycle, this pair of redox peaks still exists, indicating that the surface redox reaction is reversible. In the subsequent cycles, the curves gradually tend to overlap, indicating that the material has better cycle stability. The electrochemical performance of the material was further evaluated by the galvanostatic charge–discharge (GCD) test. As shown in Fig. 3c, at a current density of 28 mA/g (0.1 C), the first charging specific capacity of Tea-1100-NP is 326.1 mAh/g, and the ICE is 90%. After two cycles of activation at this current, continue to charge and discharge at a current density of 280 mA/g. In the subsequent cycles, the GCD curves almost overlap, indicating that Tea-1100-NP has good stability. Similar to typical hard carbon, Tea-1100-NP has two distinct voltage regions: the slope is greater than 0.1 V, and the plateau is less than 0.1 V. According to the second discharge curve, it is determined that the specific capacity contributed by the slope and platform area are 200 and 126 mAh/g, respectively. Tea-1100 also shows a similar charging and discharging process (Fig. S5a in Supporting information), but at a current density of 28 mA/g, the first charge specific capacity is only 260 mAh/g, and the ICE is 86%. Compared with the undoped Tea-1100 electrode, the charge capacity contributed by the Tea-1100-NP electrode from the slope area is increased by about 46 mAh/g. According to the "adsorption-intercalation" storage mechanism of Na^+ in hard carbon, the increase in the capacity of the ramp region may be largely related to the increase in defect sites caused by the co-doped of N, P [47]. It is worth mentioning that Tea-1100-NP has higher ICE than Tea-1100. This may be caused by the increasing number of closed micropores and carbonyl groups in the carbon framework due to re-carbonization during doping [48,49]. Fig. 3d shows the cycle performance of Tea-1100 and Tea-1100-NP for Na^+ storage, the curve shows that both electrodes exhibit stable cycle performance, however, after 100 cycles of 280 mA/g, the reversible specific capacity of the Tea-1100 electrode is only 201.4 mAh/g, through N,P co-doped, we observe that the electrochemical performance of the Tea-1100-NP electrode is improved, and the reversible specific capacity of 262.4 mAh/g is still maintained after 100 cycles of 280 mA/g, which can be attributed to the number of highly active C–P and C–N bonds and the larger interlayer spacing [50]. As mentioned earlier, in the discharge process of Tea-1100-NP, the discharge curve can be roughly divided into a slope and a gradually decreasing platform. The platform corresponds to the Na^+ insertion, and the slope area corresponds to the capacitive process. As shown in Fig. 3e, with the increase of the current

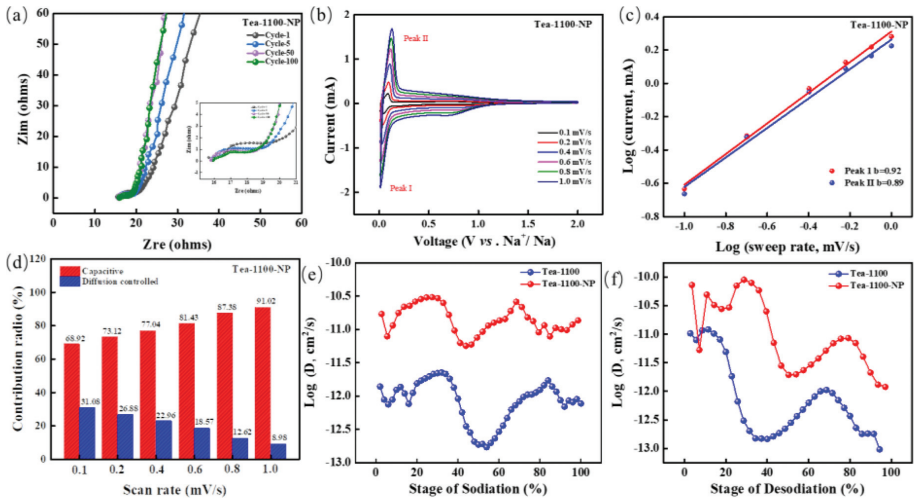

Fig. 4. (a) Tea-1100-NP of EIS analyses, the inset is the corresponding enlarged image. (b) CV curves at various scan rates. (c) The measurement of *b*-value. (d) Contribution ratio of capacitive capacities at different scan rates. (e) Sodium-ion diffusion coefficients calculated of the Tea-1100 and Tea-1100-NP electrodes for discharge. (f) Sodium-ion diffusion coefficients calculated of the Tea-1100 and Tea-1100-NP electrodes for charge.

density, the specific capacity of the Tea-1100-NP electrode from the platform area decreases rapidly, it can also be observed on the Tea-1100 electrode (Fig. S5b in Supporting information), indicating that Na^+ is inserted between the graphite layers, the kinetics is worse than the kinetics of surface adsorption on the active center. In addition, we also compared their Na^+ storage rate performance, as shown in Fig. 3f, the reversible specific capacities of Tea-1100-NP at 0.1 C, 0.2 C, 0.5 C, 1 C, 2 C and 5 C are 321.6 mAh/g, 295.8 mAh/g, 281.0 mAh/g, 268.0 mAh/g, 251.5 mAh/g and 224.5 mAh/g, respectively. In order to verify the cycling stability of our electrodes, the long-term cycling performance of two electrodes at a large current density of 5 A/g is provided (Fig. 3g), the reversible specific capacity for Tea-1100-NP electrode of 77.2 mAh/g is still maintained after 3000 cycles still maintains stable performance after 3000 cycles, and the capacity retention rate is 69%.

In order to study the improvement of the rate performance of Na^+ storage, we evaluated the EIS of the electrode. As shown in Fig. 4a, Tea-1100-NP exhibits a smaller semicircle at the intermediate frequency, indicating that the charge transfer is small after the formation of the SEI layer, there is almost no change in the interface charge transfer resistance, indicating that the SEI layer is very thin and formed very firmly, which strongly confirms the above CV results. The formation of a thin and strong SEI layer not only suppresses the loss of active materials, but also promotes the movement of Na^+ and provides excellent rate performance. In addition, it stabilizes the structure of carbon materials and provides excellent cycle stability [51,52]. CV is the main method to reveal the storage mechanism of sodium ions in carbon plates. As we all know, the storage mechanism of Na^+ includes surface capacitance behavior and bulk diffusion control process, therefore, we conducted CV tests on Tea-1100-NP at different scan rates (Fig. 4b), current (i) and scan rate (ν) obey the law [53,54]:

$$i = a\nu^b \tag{1}$$

$$\log(i) = b\log(\nu) + \log(a) \tag{2}$$

Among them, a and b are variables, and the value of b can be calculated by the relationship between $\log(i)$ and $\log(\nu)$. Generally, the value of b varies from 0.5 to 1.0. When the value of b is close to 0.5, it means that the charge and discharge process is dominated by diffusion control. When the value of b is close to 1.0, it means that the charge and discharge process is dominated by capacitance behavior, and 1.0 reveals the ideal capacitance behavior. As shown in Fig. 4c, the b values of Tea-1100-NP in the cathode and anode processes are 0.92 and 0.89, respectively, which indicates that the storage capacity of Tea-1100-NP is mainly dominated by surface adsorption capacitance. The following equation can determine the contribution rate of the capacitive behavior:

$$i = k_1\nu + k_2\nu^{1/2} \tag{3}$$

$$i/\nu^{1/2} = k_1\nu^{1/2} + k_2 \tag{4}$$

Among them, k is a constant, at a given potential, the current ($k_1\nu$) of the capacitance behavior can be determined. For example, at 1 mV/s, the capacitance contribution of Tea-1100-NP is 91.2%, as the scan rate increases, the diffusion contribution further decreases, while the capacitance contribution increases accordingly. The slow scan rate has conducive to the capacity contribution of the diffusion control process connected to the redox peak, as shown in Fig. 4d, the capacitance contributions of Tea-1100-NP at scan rates of 0.1, 0.2, 0.4, 0.6, 0.8 and 1.0 mV/s are 68.92%, 73.12%, 77.04%, 81.43%, 87.38% and 91.02%, respectively, which shows that Tea-1100-NP mainly stores Na^+ by adsorption mechanism, allowing ultrafast uptake and release of Na^+ with excellent cycling stability.

In addition, the GITT is used to calculate the diffusion coefficient (D_{Na^+}) of Na^+ in the material. The GITT data of Tea-1100 and Tea-1100-NP are obtained at a current density of 1 C for discharge 2 min followed by 1 h relaxation in the initial discharge process. According to Fick's second law, when the input current is small enough and the time interval is short sufficiently, as shows in Fig. S6a (Supporting information), the coulometric titration curve is fairly linear within the component range related in this phase, then D_{Na^+} can be calculated and following equations [55]:

$$D_{Na^+} = \frac{4}{\pi\tau}\left(\frac{m_B V_m}{M_B S}\right)^2\left(\frac{\Delta E_s}{\Delta E_\tau}\right)^2 \tag{5}$$

Among them, D_{Na^+} is the diffusion coefficient of Na^+, the unit is cm^2/s; m_B is the mass of the active material, the unit is g; V_m is the molar volume of the active material, the unit is cm^3/mol; M_B is the relative value of the positive electrode material molecular mass, the unit is g/mol; τ is the pulse time, the unit is s; ΔE_τ and ΔE_s can be obtained from the GITT curves (Fig. S6b in Supporting information), during the test process, the battery is charged with a constant current of 1 C for 1 h, during the charge process, the battery E value changes to ΔE_τ, and then the open-circuit voltage

of the battery is kept standing for 1 h to make the voltage drop to a new *quasi*-balanced potential (E_s), ΔE_s is the changes in the electrode potential during passage of the steady-state voltage. As shown in Figs. 4e and f, in the initial state, D_{Na^+} drops sharply, this is because the storage behavior of Na^+ in hard carbon materials at different potentials is divided into two types: The intercalation and release of Na^+ in the low-potential plateau area between graphite-like particles, and the second is the adsorption of Na^+ on the carbon surface and edge defects in the high-potential slope area [56]. With the gradual sodiation of the surface position, Na^+ continues to diffuse in the electrode, however, to achieve this process, Na^+ must overcome the repulsive charge gradient of Na^+ previously bound at the surface position in order to diffuse inside the electrode, so there is a sharp drop in the low potential plateau area. The plateau at lower potential below 0.1 V is attributed to the Na^+ cation insertion-extraction in the interlayers of the carbon sheets similar to that for Li^+ cation insertion–extraction in graphite [57]. The structural phase transition of GITT is consistent with the data of GITT, which further verifies the Na^+ storage mechanism of hard carbon in the low-potential plateau region. As the degree of sodiation deepens, the D_{Na^+} content gradually decreases, but the D_{Na^+} content of Tea-1100-NP is still higher than that of Tea-1100, especially higher D_{Na^+} is beneficial to improve its specific capacity. The Tea-1100-NP sample has a larger D_{Na^+}, which is advantageous in the kinetics of the charging and discharging process, which may be related to the doped of N, P and the expansion of the interlayer spacing. Therefore, the Tea-1100-NP electrode has a fast Na^+ migration rate and high Na^+ adsorption capacity, which makes it have excellent rate performance and cycle performance, which is consistent with the results of EIS and CV.

In summary, we report a scalable and versatile method to prepare N,P co-doped hierarchical porous hard carbon by simple carbonization and doped methods using the tomenta of renewable tea as a precursor. The expansion of Tea-1100-NP layer spacing and a large number of active sites are beneficial to the diffusion and transport of sodium ions and electrons. In addition, the doped of N, P modifies the surface properties of carbon, making the carbon have capacitive storage, which is faster than Na^+ intercalation. As expected, the Tea-1100-NP electrode exhibited high ICE, excellent rate performance and good cycle stability in SIB. We believe that this synthesis strategy provides a promising method, not only for the development of advanced carbonaceous materials through heteroatom doped, but also provides a new strategy for the production of low-cost and environmentally friendly electrode materials in the field of new energy.

Declaration of competing interest

The authors declare that they have no known competing financial interests or personal relationships that could have appeared to influence the work reported in this paper.

Acknowledgments

We thank the support of this work by National Natural Science Foundation of China (Nos. 21771066, 21805278, 52072323, 52122211) and the "Double-First Class" Foundation of Materials and Intelligent Manufacturing Discipline of Xiamen University. The technical assistance from the Analytical and Testing Center of Huaqiao University is likewise gratefully acknowledged.

References

[1] T. Li, C. Chen, A.H. Brozena, et al., Nature 590 (2021) 47–56.
[2] H. Au, H. Alptekin, A.C.S. Jensen, et al., Energy Environ. Sci. 13 (2020) 3469–3479.
[3] Y. Xu, C. Zhang, M. Zhou, et al., Nat. Commun. 9 (2018) 1720.
[4] J. He, C. Lu, H. Jiang, et al., Nature 597 (2021) 57–63.
[5] B. Dunn, H. Kamath, J.M. Tarascon, Science 334 (2011) 928–935.
[6] H. Liu, Z. Zhu, Q. Yan, et al., Nature 585 (2020) 63–67.
[7] K. Schutjajew, T. Tichter, J. Schneider, et al., Phys. Chem. Chem. Phys. 23 (2021) 11488–11500.
[8] C. Wang, L. Liu, S. Zhao, et al., Nat. Commun. 12 (2021) 2256.
[9] C. Vaalma, D. Buchholz, M. Weil, S. Passerini, Nat. Rev. Mater. 3 (2018) 18013.
[10] W. Zuo, X. Liu, J. Qiu, et al., Nat. Commun. 12 (2021) 4903.
[11] E.A. Wu, S. Banerjee, H. Tang, et al., Nat. Commun. 12 (2021) 1256.
[12] Z. Hou, Y. Gao, H. Tan, B. Zhang, Nat. Commun. 12 (2021) 3083.
[13] S. Sarkar, S. Roy, Y. Hou, et al., ChemSusChem 14 (2021) 3693–3723.
[14] X. Chen, Y. Fang, H. Lu, et al., Small 17 (2021) 2102248.
[15] X. Chen, Y. Zhang, Int. J. Energy. Res. 45 (2021) 9753–9779.
[16] R. Dong, L. Zheng, Y. Bai, et al., Adv. Mater. 33 (2021) 2008810.
[17] Y.Q. Li, R. Umer, Y.A. Samad, et al., Carbon 55 (2013) 321–327.
[18] H.G. Wang, Z. Wu, F.L. Meng, et al., ChemSusChem 6 (2013) 56–60.
[19] Z.H. Wang, L. Qie, L.X. Yuan, et al., Carbon 55 (2013) 328–334.
[20] F. Wu, M. Zhang, Y. Bai, et al., ACS. Appl. Mater. Interfaces 11 (2019) 12554–12561.
[21] F. Xie, Z. Xu, A.C.S. Jensen, et al., J. Mater. Chem. A 7 (2019) 27567–27575.
[22] W. Li, M. Zhou, H.M. Li, et al., Energy. Environ. Sci. 8 (2015) 2916–2921.
[23] S. Tian, D.C. Guan, J. Lu, et al., J. Power. Sources 448 (2020) 227572.
[24] N.T. Aristote, K. Zou, A. Di, et al., Chin. Chem. Lett. 33 (2022) 730–742.
[25] Z. Li, C. Bommier, Z.S. Chong, et al., Adv. Energy Mater. 7 (2017) 1602894.
[26] J.Q. Ye, H.Q. Zhao, W. Song, et al., J. Power. Sources 412 (2019) 606–614.
[27] S. Alvin, C. Chandra, J. Kim, Chem. Eng. J. 391 (2020) 123576.
[28] C. Chen, Y. Huang, Z.Y. Meng, et al., J. Mater. Sci. Technol. 76 (2021) 11–19.
[29] D.C. Qin, Z.Y. Liu, Y.Z. Zhao, et al., Carbon 30 (2018) 664–671.
[30] G. Zheng, Q. Lin, J. Ma, et al., InfoMat 3 (2021) 1445–1454.
[31] D.Q. Chen, W. Zhang, K.Y. Luo, et al., Energy Environ. Sci. 14 (2021) 2244–2262.
[32] P.Z. Wang, X.S. Zhu, Q.Q. Wang, et al., J. Mater. Chem. A 5 (2017) 5761–5769.
[33] X. Meng, P.E. Savage, D. Deng, Environ. Sci. Technol. 49 (2015) 12543–12550.
[34] M. Dahbi, M. Kiso, K. Kubota, et al., J. Mater. Chem. A 5 (2017) 9917–9928.
[35] X.D. He, J.Y. Liao, Z.F. Tang, et al., J. Power. Sources 396 (2018) 533–541.
[36] S. Tao, W. Xu, J.H. Zheng, et al., Carbon 178 (2021) 233–242.
[37] Y. Cao, L. Xiao, M.L. Sushko, et al., Nano. Lett. 12 (2012) 3783–3787.
[38] H. Wang, J. Fu, C. Wang, et al., InfoMat 4 (2022) e12241.
[39] K. Schutjajew, J. Pampel, W. Zhang, M. Antonietti, M. Oschatz, Small 17 (2021) 2006767.
[40] M. Thommes, Pure Appl. Chem. 87 (2016) 21–25.
[41] Z.Y. Gu, J.Z. Guo, X.X. Zhao, et al., InfoMat 3 (2021) 694–704.
[42] Z. Yan, Q.W. Yang, Q. Wang, J. Ma, Chin. Chem. Lett. 31 (2020) 583–588.
[43] S.F. Huang, Z.P. Li, B. Wang, et al., Adv. Funct. Mater. 28 (2018) 1706294.
[44] X. Shi, Z. Xu, C. Han, et al., Nano Micro Lett. 13 (2020) 21.
[45] C. Li, Q. Fu, K.J. Zhao, et al., Carbon 139 (2018) 1117–1125.
[46] Qian. Zhao, Y. Meng, J. Li, X. Dan, Appl. Surf. Sci. 481 (2019) 473–483.
[47] L. Shen, S. Shi, S. Roy, et al., Adv. Funct. Mater. 31 (2020) 2006066.
[48] X. Zhang, X. Dong, X. Qiu, et al., J. Power. Sources 476 (2020) 228550.
[49] W. Deng, Y. Cao, G. Yuan, et al., ACS. Appl. Mater. Interfaces 13 (2021) 47728–47739.
[50] N. Li, Q.Y. Yang, Y.X. Wei, et al., J. Mater. Chem. A 8 (2020) 20486–20492.
[51] D.Y. Kim, O.L. Li, J. Kang, Carbon 168 (2020) 448–457.
[52] Y. Liu, Q. Liu, C. Jian, et al., Nat. Commun. 11 (2020) 2520.
[53] J.L. Xia, D. Yan, L.P. Guo, et al., Adv. Mater. 32 (2020) 2000447.
[54] J.K. Mathiesen, R. Vali, M. Harmas, et al., J. Mater. Chem. A 7 (2019) 11709–11717.
[55] X. Shi, Y. Gan, Q. Zhang, et al., Adv. Mater. 33 (2021) 2100837.
[56] S. Qiu, L.F. Xiao, M.L. Sushko, et al., Adv. Energy Mater. 7 (2017) 1700403.
[57] L. Xiao, Y. Cao, W.A. Henderson, et al., Nano Energy 19 (2016) 279–288.